Inorganica Chimica Acta 418 (2014) 15–22

Contents lists available at ScienceDirect

Inorganica Chimica Acta

journal homepage: www.elsevier.com/locate/ica

One- and two-dimensional polymerisation of homoleptic M(II)-complexes of 4′-(3-pyridyl)-2,2′;6′,2″-terpyridine in the solid state: A combined study by XRD, cyclic voltammetry, NMR and UV–Vis spectroscopies

Amlan K. Pal, Baptiste Laramée-Milette, Garry S. Hanan *

Département de Chimie, Université de Montréal, 2900 Edouard-Montpetit, Montréal, Québec H3T-1J4, Canada

ARTICLE INFO

Article history:
Received 26 December 2013
Received in revised form 25 March 2014
Accepted 15 April 2014
Available online 26 April 2014

Keywords:
Homoletic complexes
Metalloligand
Paramagnetic behaviour
Terpyridine embrace
MLCT *versus* d–d transition

ABSTRACT

Homoleptic Fe(II), Co(II), Ni(II), Cu(II) and Ru(II) complexes based on the tridentate ligand 4′-(3-pyridyl)-2,2′:6′,2″-tpy (tpy = terpyridine) have been synthesized in good yields and characterized with different techniques. Although the Fe(II) and Ru(II)-complexes exhibit diamagnetic behaviour in their solution ^{1}H NMR spectra, the Co(II), Ni(II) and Cu(II) centres displaced the ^{1}H resonances between 0 and 100 ppm. The electrochemical and spectroscopic properties of the complexes indicated that the pyridyl group exhibits electron-withdrawing character. Furthermore, a deep insight into the solid state packing of Co(II)- and Cu(II)-complexes, as their hexafluorophosphate (PF_6) salts, reveals a two-dimensional terpyridine embrace, formed by face-to-face intermolecular π–π interactions that give rise to extended sheets in two dimensions. Modification of the PF_6 anions by bulky tetraphenylborate $[BPh_4]^-$ anions totally eliminates the intermolecular interactions between cations in one dimension and an extended one-dimensional polymer is formed in the other dimension.

1. Introduction

Regulating the structural and electronic properties on transition metal complexes by ligand modification is of interest due to the fine control that can be exerted over their photophysical [1,2], redox [3], and spin-state properties [4]. The incorporation of these complexes into materials for molecular electronics [2,5] solar energy conversion [6] and artificial photosynthesis [7] is thus highly desirable. While bipyridine (bpy) based metal-binding domains are commonly used as scaffolds [8], those based on 2,2′:6′,2″-terpyridine (tpy) are advantageous due to easy one-pot syntheses of structurally and substitutionally versatile motifs. The purification of bpy-based octahedral complexes that give rise to chiral (Δ- and Λ-enantiomers) [*cis*-$M(bpy)_2X_2$] and $[M(bpy)_3]X_2$ species is a lengthy process, which is not found for $_3$-coordinated tpy-complexes. In this context, the prototype 2,2′:6′,2″-terpyridine and its derivatives are important structural components in metal-directed self-assembly [8–14] and in the field of homo/heteropolynuclear metal–organic frameworks (MOFs) with unique properties [15–16].

The "metalloligands as building blocks" method has proven to be a very successful pathway to construct large, discrete supramolecular assemblies [17–20] with versatile geometries. This method has been widely accepted by several groups because of stringent control over the products formed by means of suitably oriented and readily available donor sites on the scaffolds [21].

Reports are well documented using these metallotectons as "extended ligands", where it has been shown that in homoleptic M(II)-complexes bearing 4′-(4-pyridyl)-2,2′:6′,2″-terpyridine (4-Pytpy), the N–N distance of the pendant 4-pyridyl donors is 18 Å and can give rise to discrete structures [22]. Recently, considerable attention has been focused on crystalline supramolecular motifs that are two-dimensional nets and grids of tpy embraces formed by metal complexes $[M(tpy)_2]^{2+}$. The tpy embrace involves two complexes attracted by offset-face-to-face (off) and edge-to-face (ef) interactions by the outer pyridyl rings of the ligand [23–25].

Although complexes of 4-Pytpy have been well studied, those of 4′-(3-pyridyl)-2,2′:6′,2″-terpyridine (3-Pytpy; **L**) are less explored. The complexes $[M(3\text{-Pytpy})_2]^{n+}$ have received little attention with only $[Ir(3\text{-Pytpy})_2](PF_6)_3$ [26], $[Ru(3\text{-Pytpy})_2](PF_6)_2$ [27–29], $[Fe(3\text{-Pytpy})_2](PF_6)_2$ [28–29], $[Ni(3\text{-Pytpy})_2](BF_4)_2$ [21], catena-$[Cu(3\text{-Pytpy})_2]_n$, $n(C_4Cu_2N_4S_4)$ [30] being reported to date, and in most of the cases they have been used for construction of larger

* Corresponding author. Tel.: +1 514 343 7056; fax: +1 514 343 2468.
E-mail address: garry.hanan@umontreal.ca (G.S. Hanan).

http://dx.doi.org/10.1016/j.ica.2014.04.012
0020-1693/

assemblies. Homoleptic complexes of 3-Pytpy with first row transition metal ions, such as Co(II), Ni(II) and Cu(II), with characterization by solution NMR, cyclic voltammetry and UV–Vis spectroscopy have not been reported.

To this end, we report herein, a series of homoleptic complexes of first row divalent transition metal ions, such as Fe (**1a** and **1b**), Co (**3**), Ni (**4**), Cu (**5**) and second row divalent-Ru (**2**) with 3-Pytpy, with a general molecular formula $[(C_{40}H_{28}N_8)_2M][(X)_2]$ (where M = Fe^{II}, Co^{II}, Ni^{II}, Cu^{II}, Ru^{II}, X = PF_6, BPh_4), that form either one- or two-dimensional polymers in the solid state. The complete characterization of these complexes by diamagnetic and paramagnetic solution ^{1}H NMR, HR-MS, EA, cyclic voltammetry, UV–Vis spectroscopy, and X-ray diffraction (XRD) is included. We are also interested in the ability to switch between one- and two-dimensional structures by choice of anion, and describe such a case herein.

2. Results and discussion

Although the synthesis of the ligand 3-Pytpy has been documented elsewhere [27,31,32], it could easily be synthesized in multigram quantities using recently developed single-step one-pot condensation procedure, involving condensation of the pyridine-3-carboxaldehyde with two equivalents of 2-acetylpyridine in presence of aqueous ammonia (as a source of NH_3), to form the central pyridine ring [33]. It has also been reported that refluxing in ethanol helps to improve the yield and shortening the reaction time [28] (Scheme 1).

Complexes **1a** and **2** were synthesized using literature procedures [27,29]. Complex **1b** was synthesized adopting similar synthesis procedure as complex **1a**, the anion was metathesized to $[BPh_4]^-$ by addition of an aliquot of saturated solution of $NaBPh_4$ in water. Complexes **3**–**5** were synthesized using 2:1 stoichiometric ratio of ligand:metal in a chloroform/ethanol solution at reflux for 1–2 h.[‡] Immediate colour changes were observed that depended on the metal ion used. The complexes were metathesized to their respective PF_6^- salts by addition of an excess of saturated aqueous KPF_6 solution. Recrystallization of the complexes from hot acetonitrile–water solutions provided the analytically pure complexes in good yields.

The ^{1}H NMR spectra were obtained in CD_3CN for all of the complexes at 400 MHz, where a free rotation of the pendant 3-pyridyl ring around the C–C bond simplifies the spectra, as also observed by Ollagnier et al. [28] While **1a** and **2** are found to be diamagnetic, complexes **3**–**5** are paramagnetic and the ^{1}H signals are considerably shifted and broadened with respect to typical diamagnetic complexes, as a similar observation previously reported by Medlycott et al. in homoleptic M(II)–dpt (where M = Co, Ni, Cu and dpt = 2,4-di(2-pyridyl)-1,3,5-triazine) complexes [34].

The diamagnetic ^{1}H NMR spectra of **1a** and **2** (Fig. S1 in ESI) resemble those of low-spin Fe(II)- and Ru(II)-d^6-ions, thus indicating a high ligand field strength of that 3-Pytpy ligand in an approximately octahedral coordination environment.

Although greater downfield shifts (deshielding effect) of protons 2‴, 3″, 6‴, 3, 5‴ are observed in complex **1a** compared those of its Ru(II) analogue **2**, shielding effects are observed for proton 5 and 6 due to the higher electronegativity of Fe(II) with respect to that of Ru(II), as observed by Constable and co-workers [29]. Broad, paramagnetic signals, integrating for seven chemically distinct protons and expanding up to 100 ppm are observed in the ^{1}H NMR spectra of **3** and **4**, (Fig. S2 in ESI) albeit, two protons are missing in ^{1}H NMR spectrum of complex **5** due to the excessive broadening of signals induced by the paramagnetic Cu(II)-ion.

‡ An additional amount of water is needed to dissolve the metal salt.

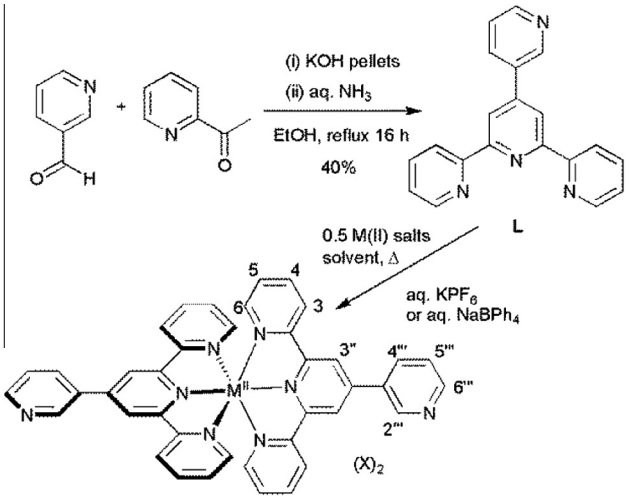

M	X	comp.	yield (%)
Fe	PF_6	1a	68
Fe	BPh_4	1b	70
Ru	PF_6	2	62
Co	PF_6	3	81
Ni	PF_6	4	80
Cu	PF_6	5	61

Scheme 1. Syntheses of ligand 3-PyTpy (**L**) and complexes **1**–**5**, with atom labeling.

2.1. Solid state structures

Although the solid state structures of cationically similar complexes, for e.g., $[C_{40}H_{28}N_8Fe]$ $[2PF_6]$ (**1a**) (CCDC 662662), $[C_{40}H_{28}N_8Ni]$ $[2BF_4]$ (CCDC 664985), catena $[C_{40}H_{28}N_8Cu]_n$, $n[C_4Cu_2N_4S_4]$ (CCDC 741499) are already reported, the anions are not the same; thereby affecting the packing environment of these structures. So, we proceeded to analyze the crystal structures of complexes **3**, **5** and examined the crystal packing of **1b** more closely with respect to that of **1a**. Specific parameters of each measurement are located in Table 1.

X-ray quality needle of **1b**, **3** and **5** were grown by slow evaporation of a saturated solution of the respective complexes in a mixture of water and acetonitrile.

Diffraction analyses reveal that all of the complexes are mononuclear and consist of the $[M(3\text{-Pytpy})_2]^{2+}$ dication and BPh_4^- (for **1b**) and PF_6^- (for **3** and **5**) counter-anions. In all of the structures, the metal atom adopts a distorted octahedral geometry in a meridional arrangement of the two tridentate terpyridine units. In the solid state structure of **1b**, (Fig. 1) the central Fe–N bonds are shorter (varies from 1.8722(13) to 1.8811(12) Å) with respect to the other four Fe–N bonds of the tpy moiety (varies from 1.9664(14) to 1.9839(13) Å). The average of bite angles subtended by the N-atoms of the individual tpy units is 162.22(5)°. These values are in close agreement to those found for $[C_{40}H_{28}N_8Fe]$ $[2PF_6]$. Both the pendant pyridine rings are twisted with respect to the pyridine ring to which they are bonded (angular separation between the least square planes containing N2 and N4, and N6 and N8 are 30.02° and 38.87°, respectively). Although in case of complex **1a** with PF_6 as the counter-anions, the two pendant pyridyl rings containing the heteroatoms are spatially separated by an angle of 47.85° in the crystal structure of **1b**, in which $[BPh_4]^-$ are the counter-anions, the pendant pyridyl rings are approximately perpendicular to each other with an interplanar separation of 88.78°, indicating a different type of packing environment in **1b** with respect to that of **1a.**

In the solid state structure of complex **1a**, the molecules are efficiently packed by two different types of offset face-to-face

Table 1
Crystal data and details of the structure determination for **1b**, **3**·2H_2O, **5**·CH_3CN.

	1b	**3**·2H_2O	**5**·CH_3CN
Formula	$[C_{40}H_{28}N_8Fe][C_{24}H_{20}B]_2$	$[C_{40}H_{28}N_8Co][PF_6]_2[2H_2O]$	$[C_{40}H_{28}N_8Cu][PF_6]_2[CH_3CN]$
Color/form	purple needle	red needle	green needle
T (K)	150(2)	150(2)	150(2)
λ	1.54178	1.54178	1.54178
Crystal system	monoclinic	monoclinic	triclinic
Space group	$P2_1/c$	$P2_1/c$	$P\bar{1}$
Unit cell dimension			
a (Å)	18.0475(12)	16.6279(5)	9.0556(6)
b (Å)	17.6434(11)	14.8960(4)	10.3716(7)
c (Å)	21.3645(14)	16.3103(5)	21.8764(14)
α (°)	90	90	84.796(4)
β (°)	102.510(3)	101.6480(10)	78.733(3)
γ (°)	90	90	73.588(3)
V (Å^3)	6641.4(7)	3956.7(2)	1931.6(2)
Z	4	4	2
$R_1(F)$; $wR(F^2)[I > 2\sigma(I)]$	0.0388; 0.1077	0.0341; 0.0899	0.0566; 0.1381
$R_1(F)$; $wR(F^2)$ (all)	0.0403; 0.1102	0.0394; 0.0931	0.0857; 0.1483
Goodness-of-fit (GOF) on F^2	1.045	1.052	0.891
Flack parameter	n.a.	n.a.	n.a.

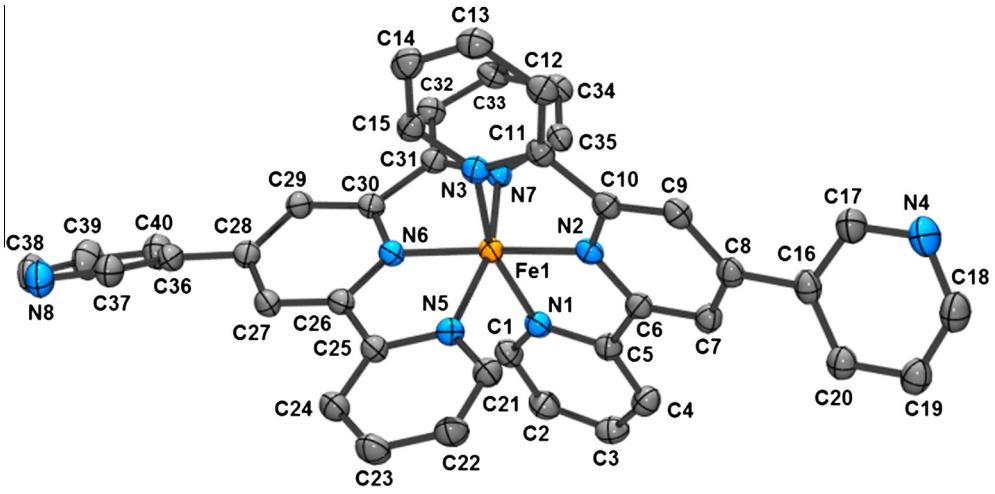

Fig. 1. Perspective view of [(**1b**)$^{2+}$], showing the labelling scheme. Thermal ellipsoids are drawn at 50% probability level. Anions and hydrogen atoms are omitted for clarity. Selected bond distances and angles: Fe1–N1 = 1.9664(14) Å, Fe1–N2 = 1.8722(13) Å, Fe1–N3 = 1.9698(12) Å, Fe1–N5 = 1.9839(13) Å, Fe1–N6 = 1.8811(12) Å, Fe1–N7 = 1.9750(12) Å, N1–Fe1–N2 = 80.96(5)°, N2–Fe1–N3 = 81.33(5)°, N5–Fe1–N6 = 81.46(5)°, N6–Fe1–N7 = 80.86(5)°, N1–Fe1–N3 = 162.13(5)°, N5–Fe1–N7 = 162.31(5)°.

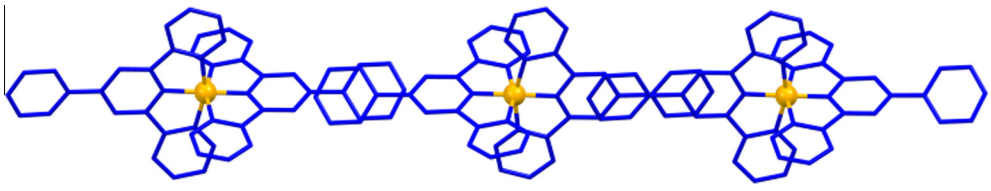

Fig. 2. Packing diagram of **1a**, showing the offset face-to-face (OFF) π–π interactions (drawn using the crystal data in ref 29).

(OFF) π–π interactions (Figs. 2 and 3): (a) interactions between two pendant pyridyl groups of two different molecules and (b) interactions between one pendant pyridyl group of one molecule and the central pyridyl unit of another molecule to form a 2D-layer. Surprisingly, in the packing structure of **1b**, (Fig. 4) no intermolecular π–π interactions were observed, rather the molecules are held together by non-classical hydrogen bonding interactions between aromatic hydrogen atoms and the N-atom of the pendant pyridyl groups with a distance of 2.71 Å. The bulky $[BPh_4]^-$ anions are strongly involved in the crystal packing by efficient onset face-to-face π–π interactions with the cationic moieties. These interactions reduce the dimensionality of the cation–cation interactions from two to one.

In the solid state structure of **3**, (Fig. 5) once again the central Co–N bonds are found to be shorter (varies from 1.9306(16) to 1.9728(17) Å) with respect to the other four Co–N bonds of the tpy moiety (varies from 2.0472(17) to 2.1761(16) Å). The average bite angles subtended by the N-atoms of the individual tpy units is 155.81(7)°, which is ~6° less than that found for **1b**. Intermolecular hydrogen bonding with co-crystallized water molecules with the two pendant pyridyl rings generate different angular relationships than those found in **1b**. The angle between the least squares

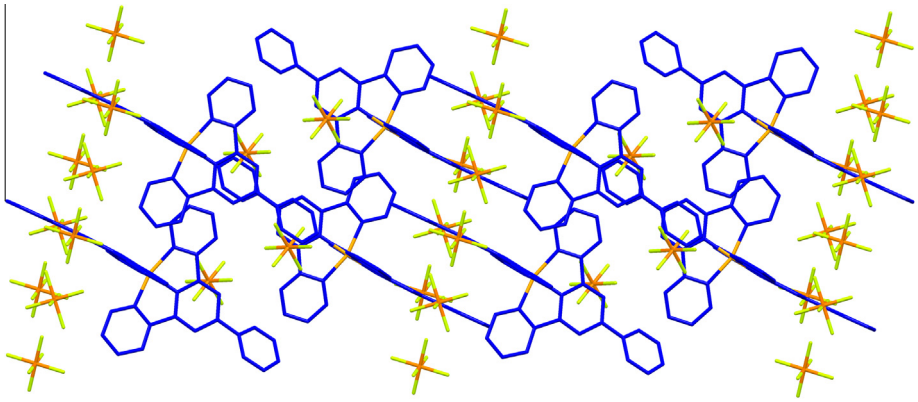

Fig. 3. Packing diagram of **1a** in 2D showing the offset face-to-face (OFF) π–π interactions to form layered structure (drawn using the crystal data in ref 29).

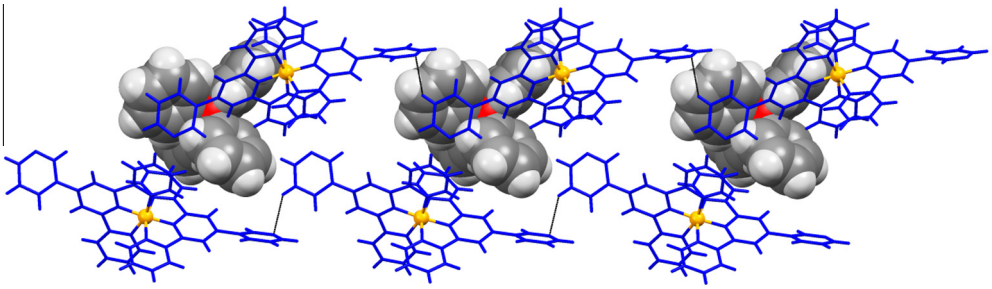

Fig. 4. Part of the infinite 1D-ribbon of **1b**, developed by non-classical H-bonding between aromatic hydrogen atoms and N-atom of the pendant pyridyl groups (black lines). The $[BPh_4]^-$ anions are involved in face-to-face onset π–π interactions with the pendant pyridyl groups.

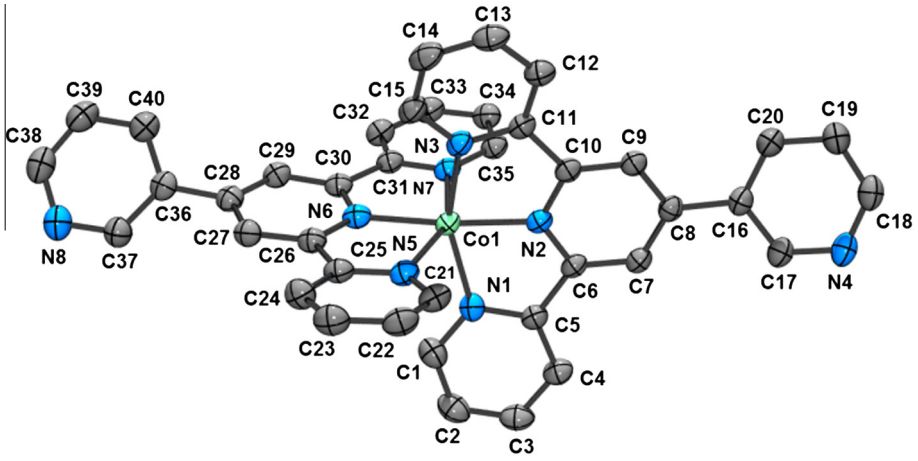

Fig. 5. Perspective view of complex **3**, showing the labelling scheme. Thermal ellipsoids are drawn at 50% probability level. Anions, hydrogen atoms and solvated water molecules are omitted for clarity. Selected bond distances and angles: Co1–N1 = 2.0511(17) Å, Co1–N2 = 1.9306(16) Å, Co1–N3 = 2.0472(17) Å, Co1–N5 = 2.1719(17) Å, Co1–N6 = 1.9728(17) Å, Co1–N7 = 2.1761(16) Å, N1–Co1–N2 = 78.72(6)°, N2–Co1–N3 = 79.26(7)°, N5–Co1–N6 = 77.30(6)°, N6–Co1–N7 = 78.12(7)°, N1–Co1–N3 = 156.27(7)°, N5–Co1–N7 = 155.34(7)°.

planes consisting of the twisted pyridyl group containing N8 and the ring containing N6 atom is 19.55° and the same angle between the planes containing N4 and N2 is 45.92°. The fact that the hetero-atoms on the pendant pyridyl groups point in the same direction with a vectorial angular separation of 60°, in turn, opens up a possibility to construct multinuclear discrete supramolecular architectures using a *trans*-directing metal-binder, for example, $PdCl_2$. Thus, the metal complex could be thought as an extended version of 3,3′-bipyridine, where the end-to-end distance (C18–C38) is 17.71 Å.

The packing of complex **3** (Fig. S1 in ESI) is supported by intermolecular hydrogen bonding between the H-atom of water with the N-atom of the pendant pyridyl groups as well as between the oxygen atom of water and H-atom of the peripheral pyridine group of the tpy unit.

X-ray structural analysis of complex **5** (Fig. 6) revealed a distorted octahedral geometry around Cu(II)-ion, with similar trends in bond distances as reported earlier for complexes **1b** and **3**. The angle between the least-square's plane containing N8 atom and the same containing N6 atom is 36.95°, whereas the least-square's

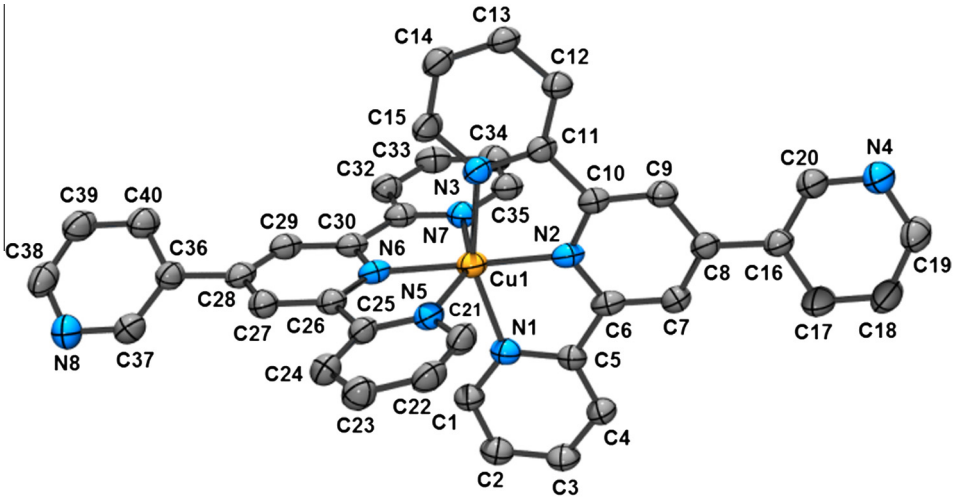

Fig. 6. Perspective view of complex **5**, showing the labelling scheme. Thermal ellipsoids are drawn at 50% probability level. Anions, hydrogen atoms and solvated water molecules are omitted for clarity. Selected bond distances and angles: Cu1–N1 = 2.090(3) Å, Cu1–N2 = 1.947(3) Å, Cu1–N3 = 2.113(3) Å, Cu1–N5 = 2.262(3) Å, Cu1–N6 = 2.012(3) Å, Cu1–N7 = 2.218(3) Å, N1–Cu1–N2 = 78.95(12)°, N2–Cu1–N3 = 78.87(12)°, N5–Cu1–N6 = 75.66(11)°, N6–Cu1–N7 = 77.13(11)°, N1–Cu1–N3 = 157.82(12)°, N5–Cu1–N7 = 152.59(11)°.

plane containing N4 is twisted by 21.17° from the least square plane containing the N2 atom. The least-square's planes containing the two pendant pyridyl substituents are separated from each other by 31.19°. In the solid state, the heteroatoms in the pyridyl groups adopt a *transoid*-configuration.

In the solid state, the molecules pack over one another efficiently due to aromatic π–π interactions (Fig. S2). Two different types of π–π interactions are observed: (i) the pendant pyridyl group of a molecule is involved in π-interactions with the pendant pyridyl group of another molecule with inter-planar distances of 4.14 Å and (ii) the pendant pyridyl group of one molecule is involved in π-interactions with one of the outer pyridyl groups of the tpy core, with inter-planar distances of 3.88 Å. Weak, but extensive, electrostatic interactions among the aromatic hydrogen atoms and aromatic π-cloud also contribute significantly to the overall crystal packing of **5**.

2.2. Electrochemistry

The electrochemical parameters of complexes **1a**, **2**–**5** were measured in dry, degassed acetonitrile using tetrabutylammonium hexafluorophosphate as the supporting electrolyte and glassy carbon electrode as working electrode and ferrocene as the internal standard. The data (reported *versus* SCE) are gathered in Table 2, although the electrochemical behaviour of complexes **1a** and **2** are already documented [29]. In all the cases the redox processes were found to be monoelectronic. Quasi-reversible metal-based oxidations are observed within 1.2–1.4 V range, however the Ru(III)/Ru(II) (Fig. 7) appears to be ~130 mV more positive than the same of Fe(III)/Fe(II) couple, which is also observed in their prototypes $[M(tpy)_2]^{n+}$ [35,36]. This result supports the red-shifting of the lowest energy ^{3}MLCT maxima of complex **1a** compared to the same of **2**, in their respective electronic absorption spectroscopies (Fig. 7).

Table 2
Redox data of complexes **1a**, **2**–**5** in dry, degassed acetonitrile.

Compound	$E_{1/2}^{Ox/v}$ (mV)[a]	$E_{1/2}^{Red/v}$ (mV)[a]			
1a	1.22(60)	−1.13(85)	−1.25(74)	−1.87(122)	–
2	1.35(86)	−1.16(61)	−1.38(88)	−1.80(104)	–
3	0.48(100)	−0.51(64)	−1.32(63)	−1.65(67)	−1.96(93)
4	1.73(irr)[b]	−1.18(71)	−1.39(98)	−1.93(138)	−2.17(150)
5	–	−0.23(65)	−0.83(irr)[b]	−1.94(110)	–

[a] Potentials are in volts *vs.* SCE for acetonitrile solutions, 0.1 M in $TBAPF_6$, recorded at 25 ± 1 °C at a sweep rate of 50 mV/s, using ferrocene as internal standard. The difference between cathodic and anodic peak potentials (millivolts) is given in parentheses. All the compounds are recorded as their hexafluorophosphate salts in their divalent states.

[b] Irreversible; potential is given for the cathodic wave.

In complex **3**, the $Co^{II/III}$ couple is quasi-reversibly centered at approximately +0.48 V, which is 210 and 240 mV more positive than $Co(tpy)_2^{3+}/Co(tpy)_2^{2+}$ and $Co(tolyl\text{-}tpy)_2^{3+}/Co(tolyl\text{-}tpy)_2^{2+}$ couples [35,37], respectively, due to the presence of electron-withdrawing pendant 3-pyridyl moiety. This value is also 100 and 60 mV more positive than $Co(Cl\text{-}tpy)_2^{3+}/Co(Cl\text{-}tpy)_2^{2+}$ and $Co(CH_3O_2S\text{-}tpy)_2^{3+}/Co(CH_3O_2S\text{-}tpy)_2^{2+}$ couples [37], respectively, suggesting that the 3-pyridyl group is more electron withdrawing than the chlorine-atom or CH_3O_2S-group. The quasi-reversible nature of this peak may be due to almost equal or slower electron self-exchange rate between Co(II) and Co(III) compared to the electron transfer rate between the cobalt ions and the electrode surface [37]. The electron self-exchange rate between Co(II) and Co(III) is delayed because of a change in electronic spin states, where Co(III) would favour the low-spin state while Co(II) may be a mixture of both spin states. In contrast, the oxidation potential is ~280 mV less positive compared to homoleptic $Co(Ph\text{-}dpt)_2^{3+}/Co(Ph\text{-}dpt)_2^{2+}$ (where Ph-dpt = 2,4-di(2′-pyridyl)-6-(phenyl)-1,3,5-triazine) [38], due to the electron withdrawing nature of the triazine core.

The cathodic region is rich with several one-electron reduction phenomena, amongst which the first reversible reduction could be assigned to Co^{II}/Co^{I} couple, which appears at ~90 mV more negative compared to $Co(Ph\text{-}dpt)_2^{3+}/Co(Ph\text{-}dpt)_2^{2+}$ system due to the relatively electron rich tpy core instead of an electron-deficient triazine moiety. The other reductions, which are also ligand-based, follow the same trend when compared to $Co(Ph\text{-}dpt)_2(PF_6)_2$.

In the absence of sufficient electrochemical data of Ni(II)–polypyridyl complexes in the literature, in complex **4**, the irreversible peak centered around +1.73 V may be assigned to oxidation of Ni(II) to Ni(III). In the cathodic region the first three quasi-reversible peaks could be assigned to the ligand-based reductions and an irreversible peak at ~−2.17 V is attributed to the reduction of Ni(II), which is ~700 mV more negative than that of Ni(II) in a homoleptic complex with Br-Ph-dpt (where Br-Ph-dpt = 2,4-di(2′-pyridyl)-6-(*p*-bromophenyl)-1,3,5-triazine), due to the significantly higher

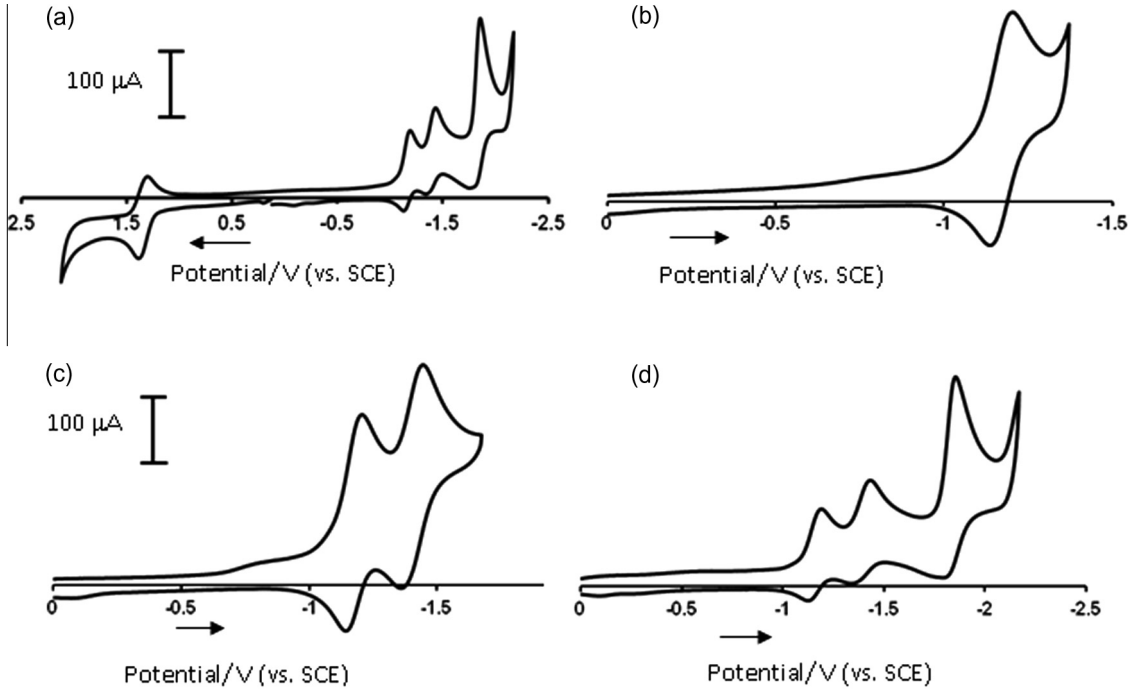

Fig. 7. Cyclic voltammogram (a) of **2** at 50 mV/s in dry, degassed acetonitrile with 0.1 (M) $TBAPF_6$ at ambient temperature with magnified views of first reversible reduction (b); first and second (quasi-) reversible reductions (c); first, second and third (quasi-) reversible reductions (d).

Table 3
Electronic absorption data of complexes **1a**, **2**–**5** in dry, degassed acetonitrile.

Compound	λ_{max}, nm ($\varepsilon \times 10^3$, M^{-1} cm^{-1})							
1a	244(40)	278(77)	285(92)	322(53)	367(7)	–	566(27)	–
2	241(38)	277(80)	283(78)	312(70)	–	–	488(28)	–
3	247(38)	285(48)	311(20)	324(19)	412(1.5)	460(1.4)	517(1.0)	682(0.01)
4	249(23)	284(48)	315(17)	327(17)	341(15)	–	–	–
5	226(51)	245(48)	280(54)	287(54)	328(16)	343(12)	668(0.05)	760(0.04)
L[a]	245.5	277	–	–	–	–	–	–

[a] From Ref. [28].

electron withdrawing effect of a dpt-core compared to a tpy-core [34].

No oxidative phenomena were observed for complex **5**, although in the cathodic region a quasi-reversible reduction at −0.23 V is observed followed by a broad reductive signal at −0.83 V. These values are consistent with the metal-based reduction as previously reported by Medlycott et al. [34] At a sufficiently negative potential a ligand-based reduction can also be observed.

2.3. UV–Vis absorption and emission spectroscopy

The electronic absorption spectra of the complexes were recorded in dry, degassed acetonitrile solution at room temperature and the absorption data are gathered in Table 3. The UV-region of the electronic spectra are dominated by ligand centered π–π^* and n–π^* transitions. While complexes **1a**, **2** and **3** are intensely coloured, complexes **4** and **5** appear to be lightly coloured, due to weak, symmetry forbidden d–d transitions in the visible and near IR regions of their absorption spectra. Complexes **1a** and **2** are intensely coloured due to an allowed metal-to-ligand charge transfer (^{1}MLCT) band in the visible region, which is characteristic for low-spin, predominantly diamagnetic complexes of d^6 metal ions. The broad ^{1}MLCT bands in the electronic absorption spectra of both **1a** and **2** can be resolved with higher energy shoulders, which may be a consequence of transitions to a tpy-based LUMO and a second, low-lying tpy based LUMO+1 in the ligand. The 3-pyridyl substituent is more electron withdrawing compared to a proton at the 4′-position of the parent tpy complex, as indicated by the *Hammett* σ parameter of 0.55 for the pendant 3-pyridyl moiety and hence the bathochromic shift in ^{1}MLCT maxima of complexes **1a** and **2**, compared to their tpy analogues (^{1}MLCT maxima of $[(tpy)_2Fe]^{2+}$ and $[(tpy)_2Ru]^{2+}$ are 548 and 475 nm, respectively) [36]. The high intensity of the colour of complex **3** (dark red) is due to several modestly absorbing MLCT transitions at a relatively higher energy region compared to complexes **4** (pale yellow) and **5** (pale green) (Fig. 8).

The electronic absorption spectra of complexes **3** and **5** are particularly interesting in terms of metal-centered d–d transitions in a tetragonally distorted ligand field, which is deviated from octahedral geometry by means of Jahn–Teller Effect, as found for low-spin Co(II) (d^7) and Cu(II) (d^9)-ions. Considering one unpaired electron in d_{z^2} orbital, as evidenced by their paramagnetic ^{1}H NMR spectrum, for complex **3**, the electron occupancy can be $(d_{xz}, d_{yz})^4$, $(d_{xy})^2$, $(d_{z^2})^1$ and thus, one would expect two different d–d transitions from $(d_{xz}, d_{yz})^4$ to $(d_{z^2})^1$ and $(d_{xy})^2$ to $(d_{z^2})^1$, with one electron orbital sequence $d_{z^2} > d_{xy} > (d_{xz}, d_{yz})$. Indeed, complex **3** exhibits two ligand field transitions centered at 517 nm and 682 nm, which may be assigned to $(d_{xz}, d_{yz})^4$ to $(d_{z^2})^1$ and $(d_{xy})^2$ to $(d_{z^2})^1$ transitions, respectively [39].

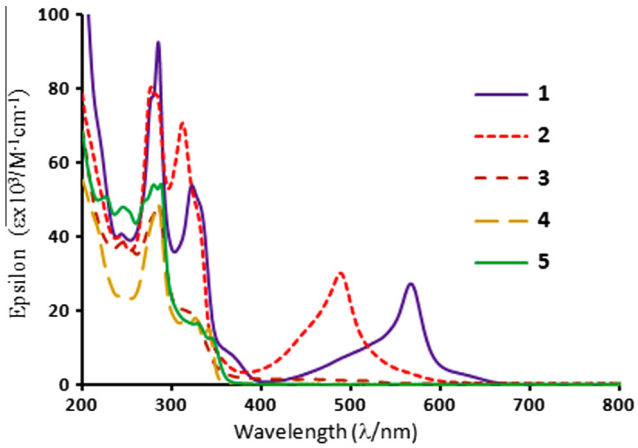

Fig. 8. Electronic absorption spectra of compounds **1a**, **2**–**5** at room temperature in deareated acetonitrile.

Following the similar arguments, the electronic configuration in d^9-Cu(II)-complex, with one electron occupancy would be $(d_{x^2-y^2})^1 > (d_{z^2})^2 > (d_{xy})^2 > (d_{xz}, d_{yz})^4$ and so, the electronic transitions centered at 668 and 760 nm could be assigned to transitions from (d_{xz}, d_{yz}) to $d_{x^2-y^2}$ and from d_{xy} to $d_{x^2-y^2}$, respectively, as observed by Nair and co-workers [39].

Emission data were recorded in dry, degassed acetonitrile solution, where only complex **2** was found to be emissive at 695 nm at ambient temperature.

3. Conclusions

A terpyridine ligand with an electron-withdrawing 3-pyridyl group has been prepared. Homoleptic 1st and 2nd row transition metal complexes in their divalent states were also synthesized. When PF_6 anions were replaced with BPh_4 anions, two-dimensional terpyridine embraces were suppressed in the solid state packing of cation $[\mathbf{1b}]^{2+}$. UV–Vis absorption spectroscopy reveals spin-allowed ^{1}MLCT transitions for complexes **1a** and **2**, whereas complexes **3** and **5** exhibit spin-forbidden d–d transitions at relatively lower energies. The quasi-reversible metal-based oxidation and reduction could be easily achieved for complex **3**, which may allow this complex to behave as a redox mediator [39]. In the field of supramolecular chemistry, these complexes with varied intrinsic properties may find application as "metalloligands as building blocks" which behave similarly as 3,3′-bipyridine and 4,7-phenanthroline [40].

4. Experimental

4.1. Materials and instrumentation

Nuclear magnetic resonance (NMR) spectra were recorded in CD_3CN at room temperature (r.t.) on a Bruker AV400 spectrometer at 400 MHz for ^{1}H NMR and at 100 MHz for ^{13}C NMR. Chemical shifts are reported in part per million (ppm). Electrochemical measurements were carried out in argon purged acetonitrile at room temperature with a BAS CV50W multipurpose potentiostat. The working electrode was a glassy carbon electrode. The counter electrode was a Pt wire, and the pseudo-reference electrode was a silver wire. The reference was set using an internal 1 mM ferrocene/ferrocinium sample at 395 mV *versus* SCE in acetonitrile. The concentration of the compounds was 1 mM. Tetrabutylammonium hexafluorophosphate (TBAP) was used as supporting electrolyte and its concentration was 0.10 M. Cyclic voltammograms were obtained at scan rates of 50, 100, 200 and 500 mV s^{-1}. For irreversible oxidation processes, the cathodic peak was used as the peak potential, and the anodic peak was used for irreversible reduction processes. The criteria for reversibility were the separation of 60 mV between cathodic and anodic peaks, the close to unity ratio of the intensities of the cathodic and anodic currents, and the constancy of the peak potential on changing scan rate. The number of exchanged electrons was measured with oscillating square wave voltammetry (OSWV), and by taking advantage of the presence of ferrocene used as the internal reference.

Experimental uncertainties are as follows: absorption maxima, ±2 nm; molar absorption coefficient, 10%; redox potentials, ±10 mV; emission maxima, ±2 nm.

4.2. Crystal structure determination

X-ray crystallographic data for **1b**, **3** and **5** were collected from a single crystal sample, which was mounted on a loop fiber. Data were collected using a Bruker Platform diffractometer, equipped with a Bruker SMART 4K Charged-Coupled Device (CCD) Area Detector using the program SMART and a rotating anode source Cu Kα radiation at 150 K. Empirical adsorption corrections were applied using the SADABS program. The structures were solved by direct method and refined using full-matrix least squares on F^2 using the SHELXTL suite of programs [41]. All non-H atoms were refined by full-matrix least-squares with anisotropic displacement parameters. The H-atoms were included in calculated positions and treated as riding atoms: aromatic C–H 0.95 Å with $U_{iso}(H) = k \times U_{eq}$ (parent C-atom), where $k = 1.2$ for the aromatic H-atoms. Structures have been analysed using MERCURY version 3.3 [42]. CCDC reference numbers 962834–962836.

4.3. Syntheses of ligand and complexes

Metal salts and other chemicals (Aldrich) were used as supplied. Ligand 3-PyTpy was synthesized by a modified literature method, in refluxing ethanolic condition [33].

4.3.1. Bis-[4′-(3-pyridyl)-(2,2′:6′,2″-terpyridine)]iron(II) tetraphenylborate, $[(C_{40}H_{28}N_8)_2Fe][(BPh_4)_2]$

Synthesized following previously published procedure [29], and the chloride salt was metathesized to $[BPh_4]^-$ salt by addition of excess aqueous $NaBPh_4$ and recrystallized from a mixture of 1:2 (v/v) acetonitrile:water. Yield 70%. ^{1}H NMR (400 MHz, acetonitrile-d_3) δ/ppm: 9.49 (s., 1 H), 9.18 (s., 2 H), 8.91 (br. s., 1 H), 8.60 (m., 3 H), 7.89 (br. s., 2 H), 7.78 (br. s., 1 H), 7.25 (m., 8 H), 7.16 (br. s., 2 H), 7.05 (m., 2 H), 6.96 (m., 8 H), 6.82 (m., 4 H). ^{13}C{^{1}H} NMR (100 MHz, acetonitrile-d_3) δ/ppm: 161.40, 158.70, 153.96, 152.42, 149.76, 148.52, 139.79, 136.61, 136.21, 133.49, 128.33, 126.52, 126.50, 126.47, 126.45, 125.30, 124.85, 122.66. ESI-MS (in CH_3CN): calculated for $C_{64}H_{48}N_8BFe$: 995.34444; found: 995.34507 $(M-BPh_4)^+$, calculated for $C_{40}H_{28}N_8Fe$: 338.08931; found: 338.08880 $(M-2BPh_4)^{2+}$. *Anal.* Calc. for $C_{88}H_{68}N_8B_2Fe{\cdot}H_2O$: C, 79.29; H, 5.29; N, 8.41. Found: C, 79.70; H, 5.12; N, 8.47%.

4.3.2. Bis-[4′-(3-pyridyl)-(2,2′:6′,2″-terpyridine)]cobalt(II) hexafluorophosphate, $[(C_{40}H_{28}N_8)_2Co][(PF_6)_2]$

3-PyTpy (0.478 g, 1.54 mmol) and $CoCl_2{\cdot}6H_2O$ (0.183 g, 0.770 mmol) were dissolved in a mixture of $CHCl_3$ (20 mL) and acetone (20 mL) and heated to reflux for 2 h. Solvent was evaporated to dryness and the chloride salt was metathesized to the PF_6 salt by addition of saturated aqueous KPF_6 solution to the aqueous solution of the compound. The resulting dark red precipitate was collected by filtration, washed with H_2O (200 mL) and Et_2O (50 mL). The red solid was redissolved in CH_3CN:H_2O (50 mL, 1:1 v/v) and the solution was concentrated by slow evaporation of the solvent,

and a red microcrystalline precipitate was obtained. The precipitate was dried under vacuum to afford the product. Yield: 81% (0.60 g). ATR-IR (powder, cm^{-1}): 557, 640, 660, 705, 734, 745, 787, 830, 1024, 1164, 1192, 1248, 1399, 1437, 1473, 1554, 1579, 1604, 1618. ^1H NMR (400 MHz, acetonitrile-d_3) δ/ppm: 9.04 (br. s., 1 H), 9.36 (br. s., 2 H), 11.51 (br. s., 1 H), 13.76 (br. s., 1 H), 14.66 (br. s., 1 H), 33.12 (br. s., 2 H), 42.59 (br. s., 2 H), 54.74 (br. s., 2 H), 94.15 (br. s., 2 H). $^{13}C\{^1H\}$ NMR (100 MHz, acetonitrile-d_3) δ/ppm: No peak was observed due to paramagnetic nature of the compound. ESI-MS (in CH_3CN): calculated for $C_{40}H_{28}N_8PF_6Co$: 824.14052; found: 824.13968 $(M-PF_6)^+$, calculated for $C_{40}H_{28}N_8Co$: 339.58790; found: 339.58910 $(M-2PF_6)^{2+}$. *Anal.* Calc. for $C_{40}H_{28}N_8P_2F_{12}Co$: C, 49.55; H, 2.91; N, 11.56. Found: C, 49.55; H, 2.80; N, 11.49%.

4.3.3. Bis-[4′-(3-pyridyl)-(2,2′:6′,2″-terpyridine)]nickel(II) hexafluorophosphate, $[(C_{40}H_{28}N_8)_2Ni][(PF_6)_2]$

3-PyTpy (0.351 g, 1.131 mmol) and $Ni(OAc)_2{\cdot}4H_2O$ (0.141 g, 0.565 mmol) were dissolved in a mixture of ethanol–chloroform–water (50 mL, 2:2:1, v/v/v) and heated to reflux for 1 h. The solvent was evaporated to dryness and the acetate salt was metathesized to the PF_6 salt by addition of saturated aqueous KPF_6 solution to the aqueous solution of the compound. The resulting golden yellow precipitate was collected by filtration, washed with H_2O (200 mL) and Et_2O (50 mL). The red solid was redissolved in CH_3CN:H_2O (50 mL, 1:1 v/v) and the solution was concentrated by slow evaporation of the solvent, and a golden microcrystalline precipitate was obtained. The precipitate was dried under vacuum to afford the product. Yield: 80% (0.44 g). ATR-IR (powder, cm^{-1}): 497, 555, 615, 634, 659, 693, 711, 747, 787, 833, 1019, 1164, 1194, 1248, 1399, 1437, 1473, 1556, 1574, 1605. ^1H NMR (400 MHz, acetonitrile-d_3) δ/ppm: 8.17 (br. s., 1 H), 11.44 (br. s., 1 H), 13.49 (br. s., 2 H), 43.71 (br. s., 1 H), 66.99 (br. s., 1 H), 74.37 (br. s., 1 H). $^{13}C\{^1H\}$ NMR (100 MHz, acetonitrile-d_3) δ/ppm: No peak was observed due to paramagnetic nature of the compound. ESI-MS (in CH_3CN): calculated for $C_{40}H_{28}N_8PF_6Ni$: 823.14267; found: 823.14335 $(M-PF_6)^+$, calculated for $C_{40}H_{28}N_8Ni$: 339.08897; found: 339.08971 $(M-2PF_6)^{2+}$. *Anal.* Calc. for $C_{40}H_{28}N_8P_2F_{12}Ni$: C, 49.56; H, 2.91; N, 11.56. Found: C, 49.27; H, 2.80; N, 11.94%.

4.3.4. Bis-[4′-(3-pyridyl)-(2,2′:6′,2″-terpyridine)]copper(II) hexafluorophosphate, $[(C_{40}H_{28}N_8)_2Cu][(PF_6)_2]$

3-PyTpy (0.231 g, 0.75 mmol) and $CuCl_2{\cdot}2H_2O$ (0.063 g, 0.37 mmol) were dissolved in a mixture of $CHCl_3$ (20 mL) and acetone (20 mL) and heated to reflux for 1 h. Solvent was evaporated to dryness and the chloride salt was metathesized to the PF_6 salt by addition of saturated aqueous KPF_6 solution to the aqueous solution of the compound. The resulting green precipitate was collected by filtration, washed with H_2O (200 mL) and Et_2O (50 mL). The green solid was redissolved in CH_3CN:H_2O (50 mL, 1:1 v/v) and the solution was concentrated by slow evaporation of the solvent, and a green microcrystalline precipitate was obtained. The precipitate was dried under vacuum to afford the product. Yield: 61% (0.22 g). ATR-IR (powder, cm^{-1}): 557, 633, 658, 706, 737, 743, 790, 832, 1021, 1054, 1164, 1196, 1248, 1400, 1438, 1475, 1554, 1576, 1594, 1619. ^1H NMR (400 MHz, acetonitrile-d_3) δ/ppm: 7.00 (br. s., 1 H), 8.87 (br. s., 1 H), 9.55 (br. s., 2 H), 9.66 (br. s., 2 H), 9.83 (br. s., 2 H). $^{13}C\{^1H\}$ NMR (100 MHz, acetonitrile-d_3) δ/ppm: No peak was observed due to paramagnetic nature of the compound. ESI-MS (in CH_3CN): calculated for $C_{40}H_{28}N_8Cu$: 341.58610; found: 341.58683 $(M-2PF_6)^{2+}$. *Anal.* Calc. for $C_{40}H_{28}N_8P_2F_{12}Cu$: C, 49.32; H, 2.90; N, 11.50. Found: C, 49.40; H, 2.83; N, 11.44%.

Acknowledgements

The authors thank the Natural Sciences and Engineering Research Council of Canada (NSERC) and Centre for Self-Assembled Chemical Structure (CSACS) for financial support.

Appendix A. Supplementary material

CCDC 662662, 664985, and 741499 contain the supplementary crystallographic data for this paper. These data can be obtained free of charge from The Cambridge Crystallographic Data Centre via www.ccdc.cam.ac.uk/data_request/cif. Supplementary data associated with this article can be found, in the online version, at http://dx.doi.org/10.1016/j.ica.2014.04.012.

References

[1] A. Juris, V. Balzani, F. Barigelletti, S. Campagna, P. Belser, A. Von Zelewsky, Chem. Rev. 84 (1988) 85. and references therein.
[2] H. Hofmeier, U.S. Schubert, Chem. Soc. Rev. 33 (2004) 373.
[3] H.C. Hurrell, H.D. Abruna, Inorg. Chem. 29 (1990) 736.
[4] E. Constable, G. Baum, E. Bill, R. Dyson, R. Eldik, D. Fernske, S. Kaderli, D. Morris, A. Neubrand, M. Neuburger, D. Smith, K. Wieghardt, M. Zehneder, A.D. Zuberbuhler, Chem. Eur. J. 5 (1999) 498.
[5] P.R. Andres, U.S. Schubert, Adv. Mater. 16 (2004) 1043.
[6] J.-P. Sauvage, J.P. Collin, J.C. Chambron, S. Guillerez, C. Coudret, V. Balzani, F. Barigelletti, L. Decola, L. Flamigni, Chem. Rev. 94 (1994) 993.
[7] J.H. Alstrum-Acevedo, M.K. Brennaman, T.J. Meyer, Inorg. Chem. 44 (2005) 6802.
[8] C. Kaes, A. Katz, M.W. Hosseini, Chem. Rev. 100 (2000) 3553.
[9] U.S. Schubert, H. Hofmeier, G.R. Newkome, Modern Terpyridine Chemistry, WILEY-VCH, Weinheim, 2006.
[10] R. Kitaura, G. Onoyama, H. Sakamoto, R. Matsuda, S.-I. Noro, S. Kitagawa, Angew. Chem., Int. Ed. 116 (2004) 2738.
[11] J.W. Steed, J.L. Atwood, Supramolecular Chemistry, second ed., John Wiley and Sons, Ltd, 2009.
[12] R. Chakrabarty, P.S. Mukherjee, P.J. Stang, Chem. Rev. 111 (2011) 6810.
[13] S. Perera, X. Li, M. Guo, C. Wesdemiotis, C.N. Moorefield, G.R. Newkome, Chem. Commun. 47 (2011) 4658.
[14] X. Lu, X. Li, J.-L. Wang, C.N. Moorefield, C. Wesdemiotis, G.R. Newkome, Chem. Commun. 48 (2012) 9873.
[15] Y.-B. Dong, M.D. Smith, H.-C. Zur Loye, Inorg. Chem. 39 (2000) 1943.
[16] S.R. Halper, L. Do, J.R. Stork, S.M. Cohen, *J. Am. Chem. Soc.* 128 (2006) 15255.
[17] P. Wang, C.N. Moorefield, M. Panzer, G.R. Newkome, Chem. Commun. 35 (2005) 4405.
[18] S.-S. Sun, A.J. Lees, Inorg. Chem. 40 (2001) 3154.
[19] M. Tominaga, S. Tashiro, M. Aoyagi, M. Fujita, Chem. Commun. 18 (2002) 2038.
[20] M. Aoyagi, K. Biradha, M. Fujita, J. Am. Chem. Soc. 121 (1999) 7457.
[21] L. Gou, L.-F. Xu, H.-M. Hu, B.-C. Wang, Q.-R. Wu, X.-L. Chen, Z.-X. Tang, Z. Anorg, Allg. Chem. 634 (2008) 1215.
[22] E.C. Constable, Coord. Chem. Rev. 252 (2008) 842.
[23] M.L. Scudder, H.A. Goodwin, I.G. Dance, New J. Chem. 23 (1999) 695.
[24] J. McMurtrie, I.G. Dance, CrystEngComm 12 (2010) 2700.
[25] (a) J. McMurtrie, I.G. Dance, CrystEngComm 11 (2009) 1141;
(b) K. Banerjee, K. Biradha, Cryst. Growth Des. 12 (2012) 4264.
[26] K.J. Arm, W. Leslie, J.A.G. Williams, Inorg. Chim. Acta 359 (2006) 1222.
[27] E.C. Constable, C.E. Housecroft, M. Neuburger, S. Schaffner, F. Schaper, Inorg. Chem. Commun. 9 (2006) 433.
[28] C.M. Ollagnier, D. Nolan, C.M. Fitchett, S.M. Draper, Inorg. Chem. Commun. 10 (2007) 1045.
[29] J.E. Beves, E.L. Dunphy, E.C. Constable, C.E. Housecroft, C.J. Kepert, M. Neuburger, D.J. Price, S. Schaffner, Dalton Trans. (2008) 386.
[30] W.-J. Shi, Online 65 (2009) m814.
[31] C.B. Smith, C.L. Raston, A.N. Sobolev, Green Chem. 7 (2005) 650.
[32] L. Persaud, G. Barbiero, Can. J. Chem. 69 (1991) 315.
[33] J. Wang, G.S. Hanan, Synlett (2005) 1251.
[34] E.A. Medlycott, K.A. Udachin, G.S. Hanan, Dalton Trans. (2007) 430.
[35] C. Arana, S. Yan, M. Keshavarz-K, K.T. Potts, H.D. Abruna, Inorg. Chem. 31 (1992) 3680.
[36] E.C. Constable, A.M.W.C. Thompson, J. Chem. Soc., Dalton Trans. (1994) 1409.
[37] J. Chambers, B. Eaves, D. Parker, R. Claxton, P.S. Ray, S.J. Slattery, Inorg. Chim. Acta 359 (2006) 2400.
[38] E.A. Medlycott, I. Theobald, G.S. Hanan, Eur. J. Inorg. Chem. (2005) 1223.
[39] V. Uma, V.G. Vaidyanathan, B.U. Nair, Bull. Chem. Soc. Jpn. 78 (2005) 845.
[40] J.R. Hall, S.J. Loeb, G.K.H. Shimizu, G.P.A. Yap, Angew. Chem., Int. Ed. 37 (1998) 121.
[41] G.M. Sheldrick, SHELXTL, 2001 and 1997, Bruker Analytical X-Ray Systems, Madison, WI.
[42] I.J. Bruno, J.C. Cole, P.R. Edgington, M.K. Kessler, C.F. Macrae, P. McCabe, J. Pearson, R. Taylor, Acta Crystallogr., Sect. B 58 (2002) 389.